

Semiconducting Sn_3O_4 nanobelts: Growth and electronic structure

O. M. Berengue,^{1,a)} R. A. Simon,¹ A. J. Chiquito,¹ C. J. Dalmaschio,² E. R. Leite,²
H. A. Guerreiro,³ and F. E. G. Guimarães³

¹*Departamento de Física, NanoLaB, Universidade Federal de São Carlos, CEP 13565-905, CP 676 São Carlos, São Paulo, Brazil*

²*Departamento de Química, Laboratório Interdisciplinar de Eletroquímica e Cerâmicas, Universidade Federal de São Carlos, CEP 13565-905, CP 676 São Carlos, São Paulo, Brazil*

³*Instituto de Física de São Carlos, Universidade de São Paulo, CEP 13560-970 São Carlos, São Paulo, Brazil*

(Received 21 August 2009; accepted 17 December 2009; published online 9 February 2010)

The study of structures based on nonstoichiometric SnO_{2-x} compounds, besides experimentally observed, is a challenging task taking into account their instabilities. In this paper, we report on single crystal Sn_3O_4 nanobelts, which were successfully grown by a carbothermal evaporation process of SnO_2 powder in association with the well known vapor-solid mechanism. By combining the structural data and transport properties, the samples were investigated. The results showed a triclinic semiconductor structure with a fundamental gap of 2.9 eV. The semiconductor behavior was confirmed by the electron transport data, which pointed to the variable range hopping process as the main conduction mechanism, thus giving consistent support to the mechanisms underlying the observed semiconducting character. © 2010 American Institute of Physics. [doi:10.1063/1.3294613]

I. INTRODUCTION

Nanowire and nanobelt based devices are at the center of the new developments in the nanoscale research. The low dimensional systems are an ideal platform to obtain an interface (building blocks) between the molecular world and useful solid state devices. Among them, oxide-based nanostructures deserve significant attention because of their unique combination of interesting structural, optical, and electronic properties, which make them a promise of smaller, faster, and cheaper nanodevices. SnO_2 is one of the most studied and used materials for the development of gas sensors,¹ transparent conductors² (high conductivity from oxygen vacancies or intentional doping), and catalysts.³ The intermediary and nonstoichiometric SnO_{2-x} ($0 < x < 1$) compounds are hardly synthesized and the fewer experimental observations are only a result of nonintentional thermal oxidation of SnO and SnO_2 phases.^{4,5} Sn_3O_4 is a good example of a nonstoichiometric structure that deserves attention. It was first identified by Lawson⁶ as a result of oxidation of another nonstoichiometric phase, SnO. Theoretically Sn_3O_4 structure should present an energy gap in the visible portion of the electromagnetic spectrum,⁷⁻⁹ which is very attractive from the view point of optical applications.^{10,11} In this way, the nonstoichiometric phases have been the subject of intense theoretical research¹² in order to study the stability of these structures and consequently to determine parameters of interest such as electronic and optical properties. In a recent work, Seko¹² used first-principles techniques and cluster expansion to calculate the most probable structure for these intermediary systems obtaining consistent data with powder diffraction. However, electron and optical properties data are still missing due to the difficulties in synthesis and in the design of devices using Sn_3O_4 as active element. Following

the literature,^{6,13} Sn_3O_4 should be present in the synthesis of SnO_2 , when SnO decomposes into Sn_3O_4 , which in turn, decomposes into SnO_2 and metallic tin. In this way, when the oxireduction process is controlled, this nonstoichiometric compound should be grown. In this paper we first report a successful approach to synthesize semiconductor single crystalline Sn_3O_4 nanobelts and the associated structural and electronic characterization.

II. EXPERIMENT

The Sn_3O_4 nanobelts were synthesized by a carbothermal evaporation process of the oxide sources.¹⁴ In the carbothermal reduction process, an oxide source to be evaporated (SnO_2 , Aldrich purity >99.99%) is mixed with carbon (Fluka, purity >99.99%) in order to allow the evaporation at low temperatures. The SnO_2 powder was mixed with graphite 95:5 in weight, respectively, by using a ball mill (Spex, CertPrep 800) for 30 min. The obtained mixture was placed in an alumina crucible and then it was inserted in an alumina tube (Lindberg Blue M), where the temperature, gas flux, and evaporation time were controlled. The optimum condition for the synthesis was 60 SCCM (SCCM denotes standard cubic centimeter per minute) N_2 flow and 600 °C for the growth temperature; the synthesis was carried out at 1200 °C for 2 h. The nanowires were characterized using a Zeiss Supra 35 FEG-SEM (FEG scanning electron microscope), a JEM 2100 transmission electron microscope, and a DMAX 2500 PC x-ray diffractometer (using Cu $K\alpha$ radiation). Raman measurements were taken using a Jobin Yvon T64000 triple grating spectrometer equipped with a liquid nitrogen cooled charge coupled device. The experiments were performed in backscattering geometry configuration and the samples were excited by a 514.5 nm line of an Ar^+ laser at room temperature (spectral resolution about 2 cm^{-1}). The devices were constructed dispersing the samples onto an oxidized n^+ Si

^{a)}Electronic addresses: olimb@df.ufscar.br and oliberengue@df.ufscar.br.

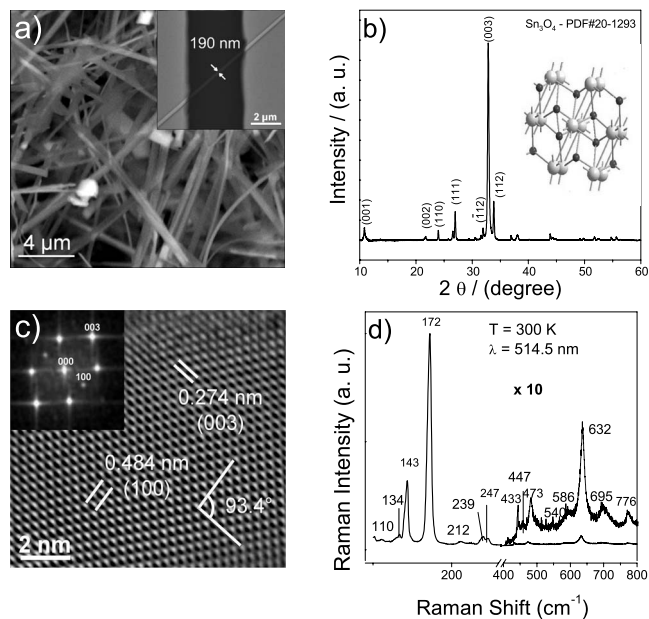


FIG. 1. Structural characterization of the Sn_3O_4 nanobelts. (a) FEG-SEM image of nanobelts: the VS mechanism is pointed as the samples' growth process. The inset shows the one-belt device used for the transport measurements. (b) The XRD pattern shows the (003) plane as the growth direction in the samples and also characterizes them as single crystals. The Sn_3O_4 lattice was found to be triclinic (PDF 20–1293) as shown in the inset. (c) HRTEM of a single Sn_3O_4 sample. It was measured two interplanar distances: (003) and (100) and the angle between these planes was found to be 93.4° in good agreement with PDF 20–1293. (d) Raman spectrum of the as-grown material taken at room temperature showing relevant phonon modes.

wafer (500 nm layer). The metallic electrodes were micro-fabricated using conventional lithographic techniques (Au/Ni, 100 nm, typical separation $L=5 \mu\text{m}$). The transport measurements were carried out at different temperatures using a closed-cycle helium cryostat Janis, CCS 350 working at a pressure lower than 5×10^{-6} Torr. The resistance data was obtained using standard low-frequency ac lock-in AMETEK 7265 detection with great noise reduction. The photocurrent (PC) measurements were obtained using a Jobin Yvon Triax 320, monochromator supplied with 2400 grating and the excitation was provided by a 500 W halogen light. The photoluminescence (PL) data were taken with a 325 nm excitation line at room temperature using a Ocean Optics HR 4000 spectrometer.

III. RESULTS AND DISCUSSION

As a first investigation of the samples, FEG-SEM measurements were performed. This analysis [Fig. 1(a)] revealed nanobelts with lateral sizes 50–240 nm and lengths of tens of micrometers.

Smooth surfaces were also found with little variation in size or shape along the wire axis. The FEG-SEM analysis provided information about the growth mechanism in our nanostructures. The absence of drops at the ends of nanobelts suggests that their growth is governed by a catalyst free process as the vapor-solid (VS) mechanism.^{14–17} As pointed out by Sun *et al.*¹⁶ SnO_2 nanostructures grew by a VS mechanism in which $\text{SnO}_2(\text{s})$ decomposes in $\text{SnO}(\text{v})$ and $\text{CO}_2(\text{v})$. The stannous oxide decomposes in $\text{SnO}_2(\text{s})$ and $\text{Sn}(\text{l})$ giving

origin to the final SnO_2 nanostructure. In the Sn_3O_4 growth, the SnO_2 nanostructures receive two layers of SnO in order to become stable and after that, a new SnO_2 layer is grown resulting in the Sn_3O_4 structure. The material's crystal structure was analyzed by x-ray diffraction (XRD). The XRD pattern was indexed as the triclinic Sn_3O_4 phase (PDF 20–1293) as observed in Fig. 1(b). The presence of a sharp and intense (003) diffraction peak indicates that the nanostructures have a preferential orientation along the [001] direction.⁹ It was also observed small quantities of SnO_2 and SnO phases which can be related to a layered growth process which occurs in this phase as discussed in a recent study.^{12,18} According to these references the nonstoichiometric compounds (SnO_{2-x}) can be seen as layered structures with SnO_2 -like and SnO-like local lattices resulting in a monoclinic lattice. In our case the Sn_3O_4 nanobelts were found to be triclinic,⁶ actually, a monoclinic lattice with small distortion angles ($\alpha=93^\circ$, $\beta=93.35^\circ$, $\gamma=91^\circ$) as observed in the inset of Fig. 1(b). The high-resolution transmission electron microscopy (HRTEM) image demonstrates the high crystallinity of a typical nanobelt [Fig. 1(c)]. The fast Fourier transform of this image [Fig. 1(c) inset] shows typical reflections of a single crystal oriented along the [010] zone axis. This analysis indicates the [001] growth direction in agreement with the XRD data, as well as the single crystal nature of the nanobelts. The samples' structure was also investigated by Raman spectroscopy. The experiments were performed in the as-grown material and the results are depicted in Fig. 1(d). The high crystalline quality of the samples is evidenced by two sharp, symmetric, and strong peaks at 143 and 172 cm^{-1} [Fig. 1(d)] which are the main phonon modes detected in Sn_3O_4 triclinic structure.^{5–9} Two sets of weak peaks in 473, 540, 632, 695, and 776 cm^{-1} and 110 and 212 cm^{-1} related to the SnO_2 rutile and tetragonal SnO structure, respectively, were also observed. Thus, the Raman data give an additional and definitive evidence for both the triclinic and layered (SnO and SnO_2) structure as suggested by XRD and HRTEM measurements. After the devices' production the electrical resistance was checked and values greater than 500 M Ω were observed, indicating an insulator behavior. In order to study this behavior, the samples' electron structure were initially characterized using room temperature PC measurements as a function of the incident energy as depicted in Fig. 2(a). The PC spectrum shows two peaks centered at ~ 430 and ~ 690 nm which can be directly related to the fundamental energy gap of the samples and to the effects of oxygen vacancies,¹⁹ respectively. Unfortunately, we are not able to distinguish the bulk and surface vacancies within our experimental setup, but as reported in the literature both kinds lead to similar results.²⁰

The observation of a gap can be considered as a first evidence of the semiconducting character of the Sn_3O_4 . From the peak at 431 nm the energy gap was estimated in 2.9 eV in the deep blue portion of the electromagnetic spectrum. This feature is very interesting for technological applications because the tin oxide stoichiometric phase shows a gap only in the ultraviolet range (3.6–4.0 eV). The peak in 689 nm can be assigned to the oxygen vacancies as stated above. Some authors^{21,22} showed the appearance of unexpected peaks in

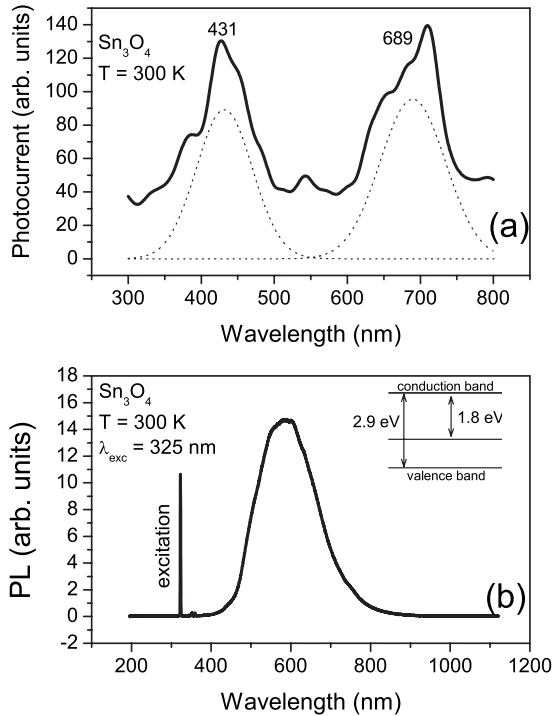


FIG. 2. PC and PL data for Sn_3O_4 nanobelts taken at room temperature. Panel (a) shows the experimental PC (solid line); the dotted lines are Gaussian fits. The peak around 431 nm is the fundamental gap of the samples while the second peak at 689 nm is related to the oxygen vacancies. In agreement with the PC results, panel (b) shows the PL spectrum with a well defined peak at 600 nm thus confirming the role of oxygen vacancies. In the inset is shown a simplified energy-band diagram of the samples.

the density of states associated with the vacancies by using both theoretical calculations and PL measurements. Then, the oxygen vacancies produce electron states in the fundamental gap leading to PL peaks at lower energies. It is interesting to add that this characteristic seems to be system independent: it appears in all metal-oxide nanostructures found in literature.²³ In this sense, our samples are also characterized by PL measurements in order to provide additional confirmation of PC results. The PL data is depicted in Fig. 2(b): a well defined peak appears around the same energy observed in the PC spectrum. As above mentioned, this result was expected and confirms the PC measurements data [the little difference between the peak position obtained from PC (689 nm) and PL (600 nm) is due to the use of one sample for PC measurements and a large amount of Sn_3O_4 belts for PL]. A more detailed investigation on the observed semiconductor character of the samples was conducted allowing the study of the mechanism(s) underlying the electron conduction process of the samples. The transport experiments were developed in dark and vacuum ($\sim 10^{-6}$ Torr) conditions because metal-oxide nanostructures are known to present a large affinity with chemical species such as O_2 molecules. In order to preserve the original characteristics of the samples we decided to avoid any optical excitation.^{11,24} Typical semiconductor current-voltage (I-V) curves as a function of temperature are depicted in Fig. 3(a).

The symmetrical I-V curves show that both the electric contacts are acting as rectifying Schottky contacts. The I-V curves show a clear (and expected) dependence on the tem-

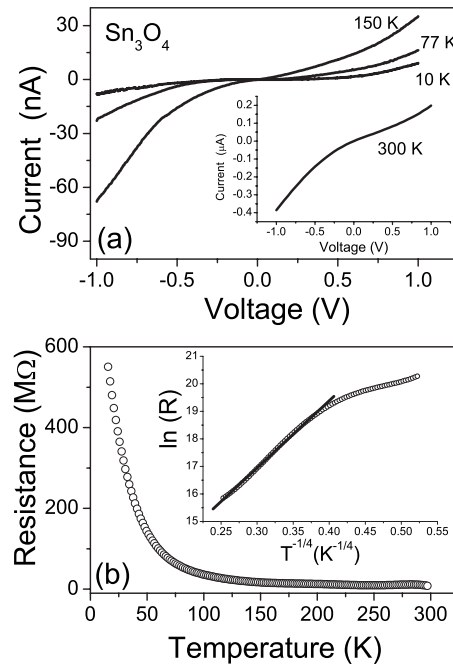


FIG. 3. Temperature dependent I-V and resistance measurements. Panel (a) clearly shows the semiconductor character of the electron transport in the Sn_3O_4 devices at different temperatures, as expected. The resistance measurements depicted in panel (b) unambiguously addresses the VRH as the physical mechanism underlying the semiconducting character of the devices.

perature. Being a semiconductor, the samples should be characterized by a well defined thermal activated process for carriers' transport which can be associated to the band conduction or to other energy states. To discuss electron transport Sn_3O_4 devices, we adopted a hoppinglike conduction as described below. The temperature-dependent resistance measurements are depicted in Fig. 3(b). The semiconductor character is then readily identified: as the temperature increases the resistance monotonically decreases over the whole temperature range. At this point we should take into account the presence of oxygen vacancies inducing both a disordered random potential and a deep level inside the gap. As a matter of fact, electrons subjected to this random potential are not able to move freely through the system if either the potential fluctuations exceed a critical value or the electron energy is lower than the characteristic value of the potential fluctuations. Taking into account these considerations, the experimental resistance data were then analyzed in the framework of the variable range hopping (VRH) process described by the well known equation²⁵

$$R = R_0 \exp\left(\frac{T_0}{T}\right)^m, \quad (1)$$

where $T_0 = \alpha\beta^3/k_B g_{(EF)}$. Here, $g_{(EF)}$ is the density of states at the Fermi level, α^{-1} is the localization length, $\beta = 5.7$, and $m = 1/4$ for the VRH process in three-dimensional systems.²⁵ In this model the localized electrons can contribute to the conduction if they experience inelastic scattering process which causes the electrons to hop from one site to another since they have similar energy. For this purpose phonons are required to conserve the energy during the hops: the higher the phonons density the bigger the carrier mobility through

localized states which cause the hopping events to grow. From the Mott theory the electron must hop a distance R_{hop} which should be greater than the localization length α^{-1} . R_{hop} can be addressed as the characteristic length associated to the carriers' transport. At a given temperature, the hopping distance R_{hop} can be calculated from

$$R_{\text{hop}} = \frac{1}{\alpha} \left(\frac{9T_0}{8\pi\beta\Gamma} \right)^{1/4}, \quad (2)$$

The fit of the Eq. (1) to the experimental data is shown in the inset of Fig. 3. The agreement between theoretical and experimental data is remarkable in a wide range of temperatures ($40 \text{ K} < T < 300 \text{ K}$) thus confirming the VRH as the main transport mechanism in the samples. The observation of this mechanism in our samples is the strongest proof of their semiconductor behavior. Moreover, from fitting results [using Eq. (2)] it was estimated the electrons' hops in 1.2 nm at 40 K (when the process starts). This length is smaller than the sample's cross section which points to a three-dimensional character of the samples for the electron transport. The above analysis is fully consistent with the optical data showing the presence of vacancy states inside the gap. The deep level generated below the conduction band bottom is large enough (1.8 eV) to prevent the electrons to be excited to the conduction states. As a consequence, the contribution of the conduction band for the electron transport is negligible in the whole range of temperature investigated.

IV. CONCLUSION

In conclusion, Sn_3O_4 single crystal nanostructures have been prepared by carbothermal evaporation of tin powders with a good reproducibility. The growth, structural, and electronic characterization of single crystalline Sn_3O_4 nanobelts was reported for the first time. It was found that the samples grow in a triclinic lattice by the VS mechanism. Also our data provide experimental evidences of a layered growth: the whole structure can be seen as alternated SnO_2 -like and SnO -like layers. By combining optical and electrical techniques, the electronic structure of the samples was experimentally investigated. PC and PL measurements provide us with the fundamental gap of the material (2.9 eV) and suggest that the oxygen vacancies induce a deep level (1.8 eV) below the conduction band that controls the observed semi-conducting VRH behavior.

ACKNOWLEDGMENTS

The authors thank Professor Alexandre J. C. Lanfredi for discussions, Professor Ariano Rodrigues for his help with the Raman apparatus, and Daniel G. Stoppa from Brazilian Synchrotron Light Laboratory for the HRTEM measurements. This work was supported by the Brazilian research funding Agencies FAPESP, CNPq, and CAPES.

- ¹V. V. Sysoev, J. Goschnick, T. Schneider, E. Strelcov, and A. Kolmakov, *Nano Lett.* **7**, 3182 (2007).
- ²Q. Wan, E. N. Dattoli, and W. Lua, *Appl. Phys. Lett.* **90**, 222107 (2007).
- ³R. Asahi, T. Morikawa, T. Ohwaki, K. Aoki, and Y. Taga, *Science* **293**, 269 (2001).
- ⁴X. Q. Pan and L. Fu, *J. Appl. Phys.* **89**, 6048 (2001).
- ⁵L. Sangaletti, L. E. Depero, B. Allieri, F. Pioselli, E. Comini, G. Sberveglieri, and M. Zocchi, *J. Mater. Res.* **13**, 2457 (1998).
- ⁶F. Lawson, *Nature (London)* **215**, 955 (1967).
- ⁷J. Geurts, S. Rau, W. Richter, and F. J. Schmitte, *Thin Solid Films* **121**, 217 (1984).
- ⁸M. Batzill and U. Diebold, *Prog. Surf. Sci.* **79**, 47 (2005).
- ⁹F. Wang, J. Zhou, T. K. Sham, and Z. Ding, *J. Phys. Chem. C* **111**, 18839 (2007).
- ¹⁰Z. L. Wang, *Annu. Rev. Phys. Chem.* **55**, 159 (2004).
- ¹¹A. J. C. Lanfredi, R. R. Geraldes, O. M. Berengue, E. R. Leite, and A. J. Chiquito, *J. Appl. Phys.* **105**, 023708 (2009).
- ¹²A. Seko, A. Togo, F. Oba, and I. Tanaka, *Phys. Rev. Lett.* **100**, 045702 (2008).
- ¹³S. Cahen, N. David, J. M. Fiorani, A. Maître, and M. Vilasi, *Thermochim. Acta* **403**, 275 (2003).
- ¹⁴E. R. Leite, J. W. Gomes, M. M. Oliveira, E. J. H. Lee, E. Longo, J. A. Varela, C. A. Paskocimas, T. M. Boschi, F. Lanciotti, Jr., P. S. Pizani, and P. C. Soares, Jr., *J. Nanosci. Nanotechnol.* **2**, 125 (2002).
- ¹⁵R. Rao, H. Chandrasekaran, S. Gubbudala, M. K. Sunkara, C. Daraio, S. Jin, and A. M. Rao, *J. Electron. Mater.* **35**, 941 (2006).
- ¹⁶S. H. Sun, G. W. Meng, M. G. Zhang, X. H. An, G. S. Wu, and L. D. Zhang, *J. Phys. D: Appl. Phys.* **37**, 409 (2004).
- ¹⁷M. O. Orlandi, E. R. Leite, R. Aguiar, J. Bettini, and E. Longo, *J. Phys. Chem. B* **110**, 6621 (2006).
- ¹⁸M. A. Mäki-Jaskari and T. T. Rantala, *Modell. Simul. Mater. Sci. Eng.* **12**, 33 (2004).
- ¹⁹H. T. Chen, S. J. Xiong, X. L. Wu, J. Zhu, and J. C. Shen, *Nano Lett.* **9**, 1926 (2009).
- ²⁰Y. C. Her, J. Y. Wu, Y. R. Lin, and S. Y. Tsai, *Appl. Phys. Lett.* **89**, 043115 (2006).
- ²¹F. Trani, M. Causà, S. Lettieri, A. Setaro, D. Ninno, V. Barone, and P. Maddalena, *Microelectron. J.* **40**, 236 (2009).
- ²²F. Trani, M. Causà, D. Ninno, G. Cantele, and V. Barone, *Phys. Rev. B* **77**, 245410 (2008).
- ²³B. Adamowicz, W. Izydorczyk, J. Izydorczyk, A. Klimasek, W. Jakubik, and J. Zywicki, *Vacuum* **82**, 966 (2008).
- ²⁴Z. Pan, Z. Dai, and Z. Wang, *Science* **291**, 1947 (2001).
- ²⁵N. F. Mott, *Metal-Insulator Transitions* (Taylor and Francis, London, 1990).